RSC Advances

ROYAL SOCIETY OF CHEMISTRY

www.rsc.org/advances

Graphical Abstract

Building smart TiO_2 nanorod networks in/on the film of P25 nanoparticles for high-efficiency dye sensitized solar cells

Yamin Feng, Jianhui Zhu, Jian Jiang, Wenwu Wang, Gaoxiang Meng, Fei Wu, Yongli Gao, Xintang Huang*

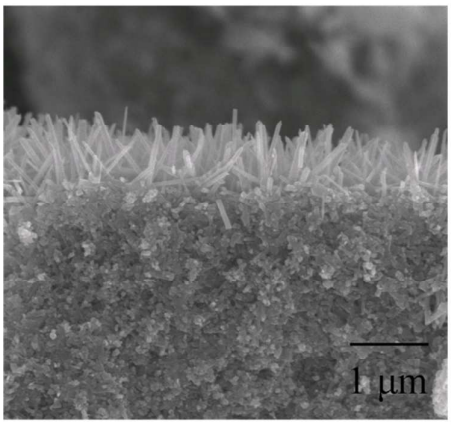

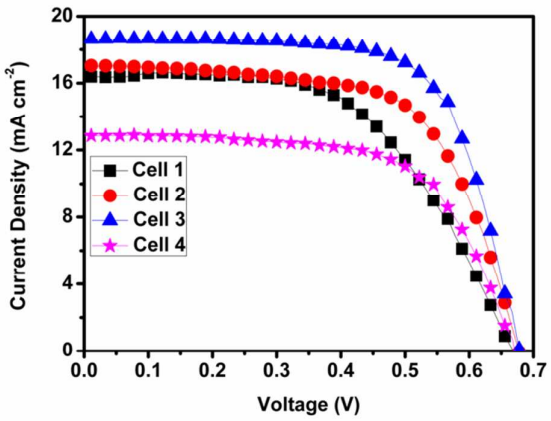

a novel hierarchical double-layered photoelectrode by integrating TiO2 nanorods (NRs) in and on the film of P25 NPs has been successfully synthesized on the FTO substrate; the hierarchical film electrodes applied in DSSCs exhibit photoelectric conversion efficiency as high as 8.62%.

Building smart TiO_2 nanorod networks in/on the film of P25 nanoparticles for high-efficiency dye sensitized solar cells

Yamin Feng, Jianhui Zhu, Jian Jiang, Wenwu Wang, Gaoxiang Meng, Fei Wu, Yongli Gao, Xintang Huang*

Institute of Nanoscience and Nanotechnology, Department of Physics, Central China Normal University, 430079, Wuhan, P. R. China.

**Corresponding author: Department of Physics, Central China Normal University, 430079, Wuhan, P. R. China.*

E-mail: xthuang@phy.ccnu.edu.cn, yaminfengccnuphy@outlook.com

Fax: +86-027-67861185

Abstract

We herein present a useful and novel strategy to redesign the photoanodes by building smart TiO_2 nanorod networks in and on the film of P25 nanoparticles (NPs) to optimize the comprehensive performance of dye-sensitized solar cells (DSSCs). By using a doctor-blade method followed by a facile hydrothermal treatment, an interesting hierarchical double-layered film consisting of P25 NPs and TiO_2 nanorods (NRs) was fabricated on fluorine-doped tin oxide (FTO) substrate. In our strategy, the P25 NPs (underlayer) with large surface area can potentially enable large amount of the dye absorption while TiO_2 NRs (overlayer) as the scatting part would effectively strengthen the light harvesting ability. Moreover, TiO_2 NRs inserted into P25 NPs film also provide conducting networks for fast photogenerated electrons transport. As demonstrated as photoanodes for DSSCs, this hierarchical double-layered photoanode indeed exhibits superior DSSCs performances to that of pure P25 NPs film; the photovoltaic conversion efficiency increases up to 8.62% under illumination of one sun (AM 1.5 G, 100 mW cm^{-2}), which is quite better than 6.12% for pure P25 NPs photoanode. This work highlights the significance of the rational design of photoanode electrodes for enhanced energy conversion applications.

Introduction

Dye-sensitized solar cells (DSSCs) have promoted intense research during the past two decades due to their low cost, simple fabrication process and relative high conversion efficiency.[1-3] A typical DSSC involves a liquid electrolyte containing I^-/I_3^-,

a Pt counter electrode, and most significantly a dye-adsorbed porous metal oxide electrode.[4-7] The efficiency of DSSCs is tightly associated with the oxide electrode and governed by the following three aspects: (i) light harvesting efficiency, (ii) electrons injection efficiency and (iii) electrons collection efficiency.[8-10] A general concept of the promotion of above efficiencies is trying to develop advanced electrode materials with high specific surface area, fast electrons transfer capability and outstanding light-scattering properties.[11-18] Though mesoporous TiO_2 nanoparticles (NPs) enable large surface area for dye loading, the great recombination loss during the photo-excited electrons collection in TiO_2 NPs severely limits the electrons diffusion coefficient and thus future commercial popularization of DSSCs.[19-23]

Fabrication of film electrodes from one-dimensional (1D) nanostructures which are capable of providing a direct electron-transport pathway has proven to be an effective way to facilitate electrons transfer.[24-26] In a film of anatase TiO_2 NPs, the electron diffusion coefficient has been demonstrated to be two orders of magnitude lower than that in single-crystal TiO_2 nanowire/nanorod.[27, 28] It is anticipated that 1D nanostructures as the photoanode electrodes could potentially facilitate electrons transport and effectively decrease the interfacial recombination, further improving the conversion efficiency.[17, 29, 30] Till now, however, the conversion efficiency of nanowire/nanorod-based DSSCs still stays at a relatively low level mainly due to the insufficient surface area for dye absorption. The state-of-art photoanodes should combine the advantages of NPs for rich dye absorption and the merits of 1D nanostructures for rapid electrons transfer, which can be hardly realized without a

smart hybrid electrode design.

In an effort to maximize the efficiency of DSSCs, we herein design a novel hierarchical double-layered photoelectrode by integrating TiO_2 nanorods (NRs) in and on the film of P25 NPs using a facile hydrothermal treatment. In this hybrid electrode design, P25 NPs with large surface area ensure the adequate dye absorption while the incorporated TiO_2 NRs can serve as not only a light-scattering scattering layer for light harvest but also electron-transport pathways that prevent the recombination of photo-electrons. The DSSC based on this hierarchical hybrid photoanode shows better performances than that of pure P25 NPs film photoanode-based DSSC. The photovoltaic conversion efficiency rises up to 8.6%, significantly higher than the value of 6.1% for the pristine P25 NPs photoanode.

Experiment

Preparation of P25 NPs film

P25 NPs film photoanode was fabricated according to the procedures mentioned in previous literatures,[31, 32] as illustrated in Scheme 1a-c. In detail, fluorine-doped tin oxide (FTO) glass sheets (15 Ω cm^{-2}) were cleaned by ultrasonication treatment in ethanol for 15 min and then immersed into an aqueous solution of 0.04 M $TiCl_4$ (Sinopharm Chemical Reagent Co., Ltd, China) at 70 ^oC for 30 min. Afterwards, the glass sheets were fetched out and kept at 60 ^oC for 20 min followed by annealed at 500 ^oC in air atmosphere for 1 h. For the preparation of the viscous paste, two kinds of pure ethyl cellulose (EC) powders, i.e., EC1 (45-55 mPa.s) and EC2 (6-9 mPa.s; 5% in

toluene:isopropanol 80:20, Aladdin Chemistry Co., Ltd.) were dissolved prior to the use of ethanol to yield 10 *wt.*% solution. Next, 0.25 g of P25 powder (Degussa AG, Germany) was mixed with 8.0 mL of ethanol (Sinopharm Chemical Reagent Co., Ltd, China) and 0.2 mL of acetic acid (99.5%, Sinopharm Chemical Reagent Co., Ltd, China) to form a sol. After 10 min of ultrasonic treatment toward the sol, 0.45 g of EC1 (45-55), 0.35 g of EC2 (6-9) of these 10 *wt.*% ethanolic mixtures and 0.3 mL of tetra-n-butyl titanate (TBT) (Tianjin fuchen Chemical Co., Ltd, China) were added to form the homogeneous paste under vigorously stirring. The obtained paste was then spread on the pre-treated FTO glasses via a doctor-blade method. The thickness of P25 NPs film can be tuned by using adhesive tapes (Scotch, 50 μm) as the spacers. After dried, the P25 NPs film was successively heated at 160 ^{o}C for 20 min, at 325 ^{o}C for 5 min, at 375 ^{o}C for 10 min, at 450 ^{o}C for 15 min, and at 500 ^{o}C for 20 min in a muffle furnace (KSL 1700X) under the air atmosphere.

Preparation of smart TiO_2 nanorod networks in and on the surface of the P25 NPs film

The hierarchical double-layered photoanode was synthesized via a facile hydrothermal method. The volume ratio of used agents (H_2O:HCl:TBT) was set as 30:30:*a* (*a*=0.4, 0.8, 1.2). Samples generated in different TBT concentration solutions were conducted by similar procedures mentioned above. In a typical synthetic procedure, 30 mL of hydrochloric acid (HCl) (37%, Sinopharm Chemical Reagent Co., Ltd, China) and 30 mL of deionized (DI) water were mixed to obtain a transparent

solution. TBT was then progressively added into the mixed solution drop by drop under vigorous agitation. After 10 min, the mixed solution was transferred into the Teflon-lined stainless steel autoclave and subsequently the P25 NPs film was also immersed into the autoclave (P25 NPs film facing down). The autoclave was sealed, put into an electric oven and maintained at 150 ^{o}C for 6 h. After the autoclave was cooled down to room temperature naturally, the samples were fetched out, rinsed with DI water several times and dried in air at 30 ^{o}C.

Characterizations

The crystallinity of P25 NPs and the hierarchical double-layered film on FTO substrate were investigated using X-ray diffraction (XRD, Bruker D8 Advance, Cu Kα radiation; λ=0.1542 nm). The surface and cross-section morphologies of all film samples were observed on a the field emission scanning electron microscopy (SEM, JEOL-6700F; 10 KV). Their light scattering properties were examined by UV-vis spectrophotometer (Model Lambda 35). Electrochemical impedance spectra (EIS) were measured by an electrochemical work station (CHI 760D, CH Instruments Inc., Shanghai) under the illumination of one sun (AM 1.5 G, 100 mW cm^{-2}) at the open circuit voltage of the cells with a frequency range from 0.1 to 100 KHz. Brunauer-Emmett-Teller (BET) surface areas (S_{BET}) measurements were estimated using BELSORP-mini (BEL Japan Inc.) with N_2 as the adsorbate at liquid nitrogen condition.

Fabrication and measurement of DSSCs

All the prepared film photoanodes were soaked in a 0.04 M $TiCl_4$ aqueous solution for 30 min at 70 ^oC followed by a sintering process at 500 ^oC in air for 30 min. After cooled down to 80 ^oC, the films were immersed into a 0.05 mM ethanol solution of N719 dye at room temperature for 24 h. A FTO substrate sputter-coated by Pt layer with a thickness of 60 nm was used as the counter electrode. The dye-sensitized photoanode together with the Pt-coated FTO glass were assembled into a sandwich-type cell. A liquid electrolyte (about 10 μL) containing0.1 M of LiI, 0.05 M of I_2, 0.5 M of 4-tertbutylpyr-idine and 0.6 M of tetrabutylammonium iodide in acetonitrile was then injected into the interspace between the dye-sensitized film electrode and the counter electrode. The edges of cells were carefully sealed by a hot-melt polymer film (Surlyn, 1702; film thickness: 60 μm). The photovoltaic measurements were performed in air by a solar simulator (Oriel, 91192) under illumination of one sun (AM 1.5 G, 100 mW cm^{-2}). For the resultant cell, the exposed area in light was approximately 0.2 cm^2. To estimate the dye adsorbed amount on photoanodes, the sensitized electrodes were separately immersed into a 1 mM of NaOH solution. Then, the absorbance of the resulting solutions was measured by a UV-vis spectrophotometer (Shimadzu UV-2450).

Result and discussion

P25 NPs films and the hierarchical films prepared in different solutions (a=0.4, 1T-P25; 0.8, 2T-P25; 1.2, 3T-P25) on FTO substrates were initially examined by XRD measurement. Fig. 1 shows that except for diffraction peaks arising from FTO glasses

(marked by square), the peaks detected from P25 NPs film can be indexed to distinct anatase (JCPDS No. 21-1272) and rutile (JCPDS No. 21-1276) TiO_2, respectively. For comparison, in the case of hierarchical films, there are new diffraction peaks appearing, which are also indexed to rutile-phased TiO_2 (JCPDS No. 21-1276; highlighted by dotted circle) and demonstrating the later successful building of TiO_2 NRs into/onto P25 NPs film via hydrothermal treatment. SEM observations on the surface and the cross-sectional morphology of P25 NPs film (See Fig. 2) and the hierarchical film (See Fig. 3) have been made. Fig. 2a displays a low-magnification SEM image of P25 NPs film, which reveals that the film is uniform with few cracks. The cross-section SEM image in Fig. 2b indicates that the thickness of P25 NPs film is about 13.5 μm. Fig. 3a-c successively show typical SEM images of the hierarchical film obtained from different reaction solutions (the added TBT volume is 0.4, 0.8, 1.2 mL). With a low concentration of TBT (about 0.4 mL), it is clear that very few TiO_2 NRs appear on either the outer surface or the inner side of P25 NPs film (Fig. 3a). Upon the addition of TBT up to 0.8 mL, there are large quantities of nanorods in a diameter range of 70-90 nm grown on the top surface of P25 film (Fig. 3b). When the introduced TBT rises to 1.2 mL, both the amount and the size of resultant nanorod products increased (up to 100~120 nm), as obviously displayed in Fig. 3c. Above results indicate that the concentration of TBT is highly associated with the hydrothermal growth of TiO_2 NRs. Fig. 3d-f display the cross-section and top-view images of the hierarchical film fabricated with a moderate TBT dosage of ~0.8 mL. Top-view SEM image of the produced hierarchical film (Fig. 3e) reveals the large-scale and uniform formation of

TiO_2 NRs on P25 film surface after the hydrothermal process. Low-magnification image also illustrates that the thickness of 2T-P25 film is ~14 μm, similar to the case of P25 NPs film (13.5 μm) in the absence of hydrothermal treatment (See Fig.S1a). An enlarged cross-section SEM observation captured from the black rectangular part of Fig.S1a has also been made. As indicated by blue circles in Fig. S1b, it is clear that TiO_2 NRs can be easily distinguished from P25 NPs indicating that smart 1D TiO_2 NRs were able to grow inside P25 NPs film. The existing TiO_2 NRs network in P25 NPs film would potentially provide direct electrons transport way and consequently reduce the recombination rate of electrons. The SEM image from the root of the hierarchical films (Fig. 3d), reveals that the TiO_2/P25 film has a good contact with the FTO film after hydrothermal treatment. Fig. 3f shows the magnified cross-section SEM observations toward the hierarchical film. It is found that the well-distinguished NRs structures with average length of around 1 μm are uniformly grown on the top of P25 NPs, illustrating that TiO_2 NRs are distributed not only in the NPs film but also on the outer surface of P25 NPs film.

UV-vis diffuse reflectance spectra were made to compare the scattering effect of all film samples. Diffuse reflectance spectra of P25 NPs film (Cell 1) and the hierarchical films (a=0.4, Cell 2; a=0.8, Cell 3; a=1.2, Cell 4) were shown in Fig. 4. Compared to pure P25 NPs film, all the hierarchical films possessed a strong scatting effect in the wavelength region of 400~800 nm. This indicates that the incorporated TiO_2 NRs in/upon P25 NPs film indeed have a better light-scattering capability than the case of pure P25 NPs film. Fig. 5 shows the photocurrent-photovoltage (*J-V*) curves of DSSCs

fabricated by P25 NPs and the hierarchical film with the similar thickness of ~13.5 μm, respectively. The corresponding photovoltaic parameters and the dye absorption results were summered in Table 1. The cell made from P25 NPs film (Cell 1) exhibits an open voltage (V_{oc}) of 0.666 V, a short circuit density (J_{sc}) of 16.20 mA cm^{-2}, a fill factor (FF) of 56.5% and conversion efficiency (η) of ~6.12%. It is interesting to note that after the hydrothermal treatment, the J_{sc} varies significantly from 16.20 mA cm^{-2} (for Cell 1) to 17.09 mA cm^{-2} (for Cell 2), 18.66 mA cm^{-2} (for Cell 3), 12.28 mA cm^{-2} (for Cell 4), respectively. The highly improved J_{sc} in Cell 2 and Cell 3 can be mainly attributed to two reasons: (i) the improved dye adsorption by the introduced TiO_2 NRs, and (ii) the enhanced light harvesting efficiency due to the strong light scattering effect of TiO_2 NRs layer (Scheme 2a), which plays a vital role for high-efficiency energy conversion.[11, 12, 33, 34] As shown in Scheme 2a, it revealed that the present of TiO_2 NRs in/upon P25 NPs film will play a vital roles for increasing the light scattering. The Cell 2 and Cell 3 obviously have a better light-scattering capability than that of Cell 1 within the same wavelength range (400~800 nm) (Fig. 4), revealing the improvement of light scattering abilities for such a kind of hierarchical films. However, the J_{sc} value of Cell 4 dramatically drops to 12.28 mA cm^{-2} (lowest). We suppose that the decrease of J_{sc} value could be mainly ascribed to its poor dye loading, mainly ascribed to its poor dye loading resulting in low charge generation. Once there are excessive TiO_2 NRs inserted, the pores in P25 NPs film were blocked or filled by NRs, subsequently hindering the dye absorption. The poor dye loading capacity for Cell 4 can be attributed to the low surface areas of the film, as verified by

Brunauer-Emmett-Teller (BET) surface area (S_{BET}) measurements. The S_{BET} of the Cell 4 is 7.79 m^2 g^{-1}, which is obviously lower than that of other cells (Cell 1: 45.08 m^2 g^{-1}; Cell 2: 76.58 m^2 g^{-1}; Cell 3: 79.14 m^2 g^{-1}). After comparing the V_{oc} value of these four type cells, it can be found that DSSCs based on the hierarchical films have a similar V_{oc} value (Cell 2: 0.678 mV ; Cell 3: 0.689 mV ; Cell 4: 0.678 mV), which is a bit higher than that of P25 film (Cell 1: 0.666 mV). As we known, the V_{oc} value of DSSCs is determined by the difference between the Fermi level for electrons in the photoanode and the redox potential of I^-/I_3^-.[21, 35, 36] As shown in Scheme 2b, due to the direct transport ways provided by smart TiO_2 NRs network inside the films of P25 NPs, the electrons transport rate is significantly increased, and hence the charge recombination is also reduced to some extent. This also leads to the enhancement of electrons density on the TiO_2 NRs/P25 surface, thus giving rise to the increase of V_{oc} and a positive shift of Fermi level. The fill factors (FFs) are measured to be 56.5% (Cell 1), 63.4% (Cell 2), 67.1% (Cell 3) and 66.1% (Cell 4), respectively. The record reflects that the FF value firstly increases with amount of incorporated TiO_2 NRs in/onto P25 NPs film but finally suffers from a slight drop. This result could be highly related to TiO_2 NRs which lower the series resistance and provide better contact between the electrolyte and titania.[26] As demonstrated, the power conversion efficiencies of our composite structured solar cells were 7.35% for Cell 2, 8.62% for Cell 3 and 5.51% for Cell 4, respectively.

Electrochemical impedance spectra (EIS) technique is a powerful characterization technology to understand the electrochemical/photoelectrochemical processes in

DSSCs. EIS spectra of the four cells was performed under the illumination of one sun (AM 1.5 G, 100 mW cm^{-2}) at the open circuit voltage of the cells. Fig. 6a and b show the Nyquist plots and the Bode curves of DSSCs assembled with P25 NPs and the hierarchical film specimens, respectively. There are two arcs observed in the Nyquist plot (Fig. 6a). The first semicircle in the high-frequency region (>1 kHz) is assigned to the redox charge transfer at the counter electrode whereas the second one occurring in the medium-frequency range (100–1 Hz) represents the electrons transfer at the oxide/electrolyte interface.[37-39] Under the V_{oc} condition, there is no current passing through the external circuit, implying the electrons injected into P25 or TiO_2/P25 were recombined with electrolyte at the TiO_2/dye/electrolyte interface.[10, 40, 41] As can be seen, after TiO_2 NRs were introduced into P25 NPs film, the charge recombination resistance of electrodes (Cell 2: 164.1 Ω; Cell 3: 289.8 Ω; Cell 4: 138.2 Ω) was higher than that of pure P25 NPs film (Cell 1: 59.2 Ω). Moreover, the Cell 3 film exhibited the largest resistance value, reflecting its capability of effectively preventing the electrons from recombination on the semiconductor-electrolyte interface. This can attributed to the fact that appropriate incorporation of smart TiO_2 NRs, thus leading to the lowest recombination rate of electrons. The Bode-phase plots (Fig. 6b) show a corresponding characteristic frequency peak. Based on the characteristic frequencies at the mid-frequency peaks value (f_{max}), the electron lifetime (τ_e) for these four DSSCs can be calculated according to the following equation.

$$\tau_{e=}\frac{1}{(2\pi f_{max})}$$

As observed in Fig. 6b, the f_{max} values are 11.85, 11.25, and 56.25 Hz for Cell 1, Cell 2

and Cell 4, respectively. The Cells 3 has the lowest f_{max} value (3.23Hz). According to the above equation, we can readily conclude that the Cell 3 has the longest τ_e. This means that electrons can transfer a longer distance to a larger extent with unblocked ways across the TiO_2-P25/dye/electrolyte interface, leading to more effective capture and collection of electrons and also confirming the function of smart TiO_2 NRs network.

Conclusion

In summary, a novel hierarchical double-layered photoelectrode was synthesized for enhanced performance of DSSCs. The double-layered photoelectrode consists of TiO_2 NRs grown either in the film or on a top surface as the scattering layers and a bottom layer of P25 NPs providing the large surface area for dye absorption. Moreover, we have also demonstrated that TiO_2 NRs inserted into the P25 NPs film can effectively function as a direct electron transport network, eventually reducing the recombination of electrons. The hierarchical double-layered electrode demonstrated a high conversion efficiency of 8.6% which was much higher than that of pure P25 NPs film (6.12%). The remarkable enhancement of the photovoltaic performance is mainly attributed to the superior light scattering ability, the faster electron transport and better dye absorption ability.

Acknowledgment

We gratefully acknowledge financial support from the National Natural Science

Foundation of China (No. 51172085).

References

1. B. O'Regan and M. Grätzel, *Nature*, 1991, **353**, 737-740.
2. M. Grätzel, *Nature*, 2001, **414**, 338-344.
3. A. Yella, H. W. Lee, H. N. Tsao, C. Yi, A. K. Chandiran, M. K. Nazeeruddin, E. W. Diau, C. Y. Yeh, S. M. Zakeeruddin and M. Grätzel, *Science*, 2011, **334**, 629-634.
4. M. Grätzel, *Chemistry Letters*, 2005, **34**, 8-13.
5. F. Odobel, Y. Pellegrin and J. Warnan, *Energy & Environmental Science*, 2013, **6**, 2041-2052.
6. Y. Li, H. Wang, Q. Feng, G. Zhou and Z.-S. Wang, *Energy & Environmental Science*, 2013, **6**, 2156-2165.
7. K. Kakiage, T. Tokutome, S. Iwamoto, T. Kyomen and M. Hanaya, *Chemical Communications*, 2013, **49**, 179-180.
8. C. Wu, W. Liao and J. Wu, *Journal of Materials Chemistry*, 2011, **21**, 2871-2876.
9. X. Zhang, V. Thavasi, S. G. Mhaisalkar and S. Ramakrishna, *Nanoscale*, 2012, **4**, 1707-1716.
10. C. Gao, X. Li, B. Lu, L. Chen, Y. Wang, F. Teng, J. Wang, Z. Zhang, X. Pan and E. Xie, *Nanoscale*, 2012, **4**, 3475-3481.
11. W. Q. Wu, Y. F. Xu, H. S. Rao, C. Y. Su and D. B. Kuang, *Nanoscale*, 2013, **5**, 4362-4369.

12. K. N. Li, Y. F. Wang, Y. F. Xu, H. Y. Chen, C. Y. Su and D. B. Kuang, *ACS Applied Materials & Interfaces*, 2013, **5**, 5105-5111.

13. W. T. Jiang, C. T. Wu, Y. H. Sung and J. J. Wu, *ACS Applied Materials & Interfaces*, 2013, **5**, 911-917.

14. L. De Marco, M. Manca, R. Giannuzzi, M. R. Belviso, P. D. Cozzoli and G. Gigli, *Energy & Environmental Science*, 2013, **6**, 1791-1795.

15. H. Wang, M. Miyauchi, Y. Ishikawa, A. Pyatenko, N. Koshizaki, Y. Li, L. Li, X. Li, Y. Bando and D. Golberg, *Journal of the American Chemical Society*, 2011, **133**, 19102-19109.

16. J. Li, H. Fan and X. Jia, *Journal of Physical Chemistry C*, 2010, **114**, 14684-14691.

17. C.-Y. Lin, Y.-H. Lai, H.-W. Chen, J.-G. Chen, C.-W. Kung, R. Vittal and K.-C. Ho, *Energy & Environmental Science*, 2011, **4**, 3448-3455.

18. G. Cheng, M. S. Akhtar, O. B. Yang and F. J. Stadler, *Electrochimica Acta*, 2013, **113**, 527-535.

19. W. Wu, J. Liao, H. Chen, X. Yu, C. Su and D. Kuang, *Journal of Materials Chemistry*, 2012, **22**, 18057-18062.

20. L. Yang and W. W. Leung, *Advanced Materials*, 2013, **25**, 1792-1795.

21. A. Hagfeldt, G. Boschloo, L. Sun, L. Kloo and H. Pettersson, *Chemical Reviews*, 2010, **110**, 6595–6663.

22. B. Weintraub, Y. Wei and Z. L. Wang, *Angewandte Chemie International Edition*, 2009, **48**, 8981-8985.

23. G. Cheng, M. S. Akhtar, O. B. Yang and F. J. Stadler, *ACS Applied Materials & Interfaces*, 2013, **5**, 6635-6642.

24. Q. Zhang and G. Cao, *Nano Today*, 2011, **6**, 91-109.

25. M. McCune, W. Zhang and Y. Deng, *Nano Letters*, 2012, **12**, 3656-3662.

26. M. Yang, S. Neupane, X. Wang, J. He, W. Li and N. Pala, *ACS Applied Materials & Interfaces*, 2013, **5**, 9809-9815.

27. Y. Bai, H. Yu, Z. Li, R. Amal, G. Q. Lu and L. Wang, *Advanced Materials*, 2012, **24**, 5850-5856.

28. L. Forro, O. Chauvet, D. Emin, L. Zuppiroli, H. Berger and F. Lévy, *Journal of Applied Physics*, 1994, **75**, 633-635.

29. Y. Feng, X. Ji, J. Duan, J. Zhu, J. Jiang, H. Ding, G. Meng, R. Ding, J. Liu, A. Hu and X. Huang, *Journal of Solid State Chemistry*, 2012, **190**, 303-308.

30. S. H. Ko, D. Lee, H. W. Kang, K. H. Nam, J. Y. Yeo, S. J. Hong, C. P. Grigoropoulos and H. J. Sung, *Nano Letters*, 2011, **11**, 666–671.

31. S. Ito, T. N. Murakami, P. Comte, P. Liska, C. Grätzel, M. K. Nazeeruddin and M. Grätzel, *Thin Solid Films*, 2008, **516**, 4613-4619.

32. C. Hsu, K. Lee, J. T. Huang, C. Lin, C. Lee, L. Wang, S. Tsai and K. Ho, *Electrochimica Acta*, 2008, **53**, 7514-7522.

33. X. Wu, G. Q. Lu and L. Wang, *Energy & Environmental Science*, 2011, **4**, 3565-3572.

34. F. Shao, J. Sun, L. Gao, S. Yang and J. Luo, *Journal of Materials Chemistry*, 2012, **22**, 6824-6830.

35. M. Wang, Y. Wang and J. Li, *Chemical Communications*, 2011, **47**, 11246-11248.

36. M. Grätzel, *Journal of Photochemistry and Photobiology C: Photochemistry Reviews*, 2003, **4**, 145-153.

37. Q. Wang, J. E. Moser and M. Grätzel, *Journal of Physical Chemistry B*, 2005, **109**, 14945-14953.

38. S. Y. Huang, G. Schlichthörl, A. J. Nozik, M. Grätzel and A. J. Frank, *Journal of Physical Chemistry B*, 1997, **101**, 2576-2582.

39. Y. Feng, F. Wu, J. Jiang, J. Zhu, G. J. Fodjouong, G. Meng, Y. Xing, W. Wang and X. Huang, *Journal of Alloys and Compounds*, 2013, **581**, 610-615.

40. Y.-Z. Zheng, X. Tao, Q. Hou, D.-T. Wang, W.-L. Zhou and J.-F. Chen, *Chemistry of Materials*, 2011, **23**, 3-5.

41. Q. Hu, C. Wu, L. Cao, B. Chi, J. Pu and L. Jian, *Journal of Power Sources*, 2013, **226**, 8-15.

Table 1 Dye loading and characteristics of the solar cells measured under illumination of one sun (AM 1.5 G, 100 mW cm^{-2}).

Cell	Dye loading (10^{-7} mol cm^{-2})	J_{sc} (mA cm^{-2})	V_{oc} (V)	FF	η (%)
Cell 1	0.79	16.20	0.666	56.5%	6.12
Cell 2	1.24	17.09	0.678	63.4%	7.35
Cell 3	1.32	18.66	0.689	67.1%	8.62
Cell 4	0.21	12.28	0.678	66.1%	5.51

Figure captions

Scheme 1 Schematic diagram showing the evolution of the TiO_2/P25 composite film; (a) a clean FTO substrate, (b) $TiCl_4$ treated FTO substrate, (c) P25 NPs film obtained from the doctor-blade method, (d) TiO_2/P25 composite film.

Scheme 2 Sketch showing light scattering in the TiO_2/P25 composite film (a) and the electron transport through the semiconductor oxide film (b).

Fig. 1 XRD patterns of P25 NPs film and TiO_2/P25 composite film on FTO substrate.

Fig. 2 (a) Top-view and (b) cross-section SEM observations of P25 NPs film.

Fig. 3 SEM images of TiO_2/P25 composite film synthesized by hydrothermal treatment with different amounts of Ti-precursor. (a) 0.4 mL, (b) 0.8 mL, (c) 1.2 mL. SEM images of 2T-P25 film from the (d-f) cross-section and (e) top view, respectively.

Fig. 4 Diffuse reflectance spectra of four-type photoanodes with P25 film (Cell 1), 1T-P25 film (Cell 2), 2T-P25 film (Cell 3), 3T-P25 film (Cell 4).

Fig. 5 J-V characteristics of DSSCs based on pure P25 NPs film and TiO_2/P25 composite photoanodes with a film thickness of ~13.5 mm.

Fig. 6 (a) Nyquist plot and (b) Bolt plot from electrochemical impedance spectra of four-type cells.

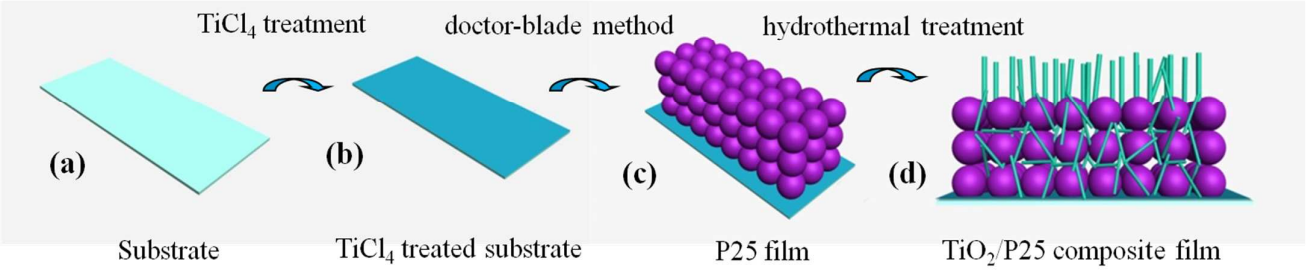

Scheme 1

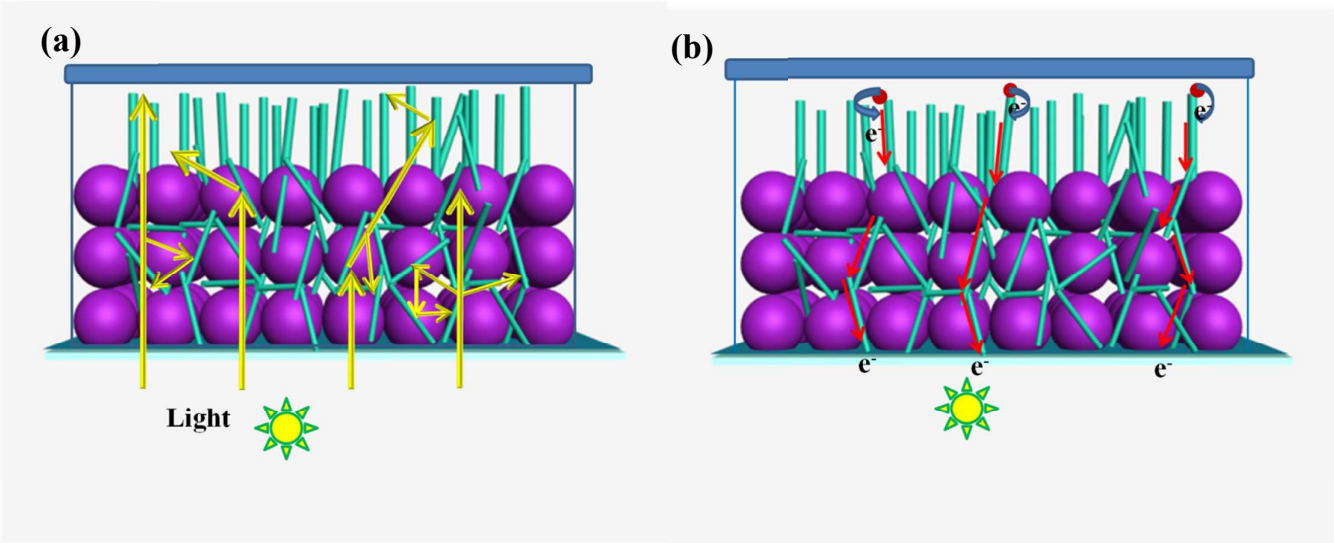

Scheme 2

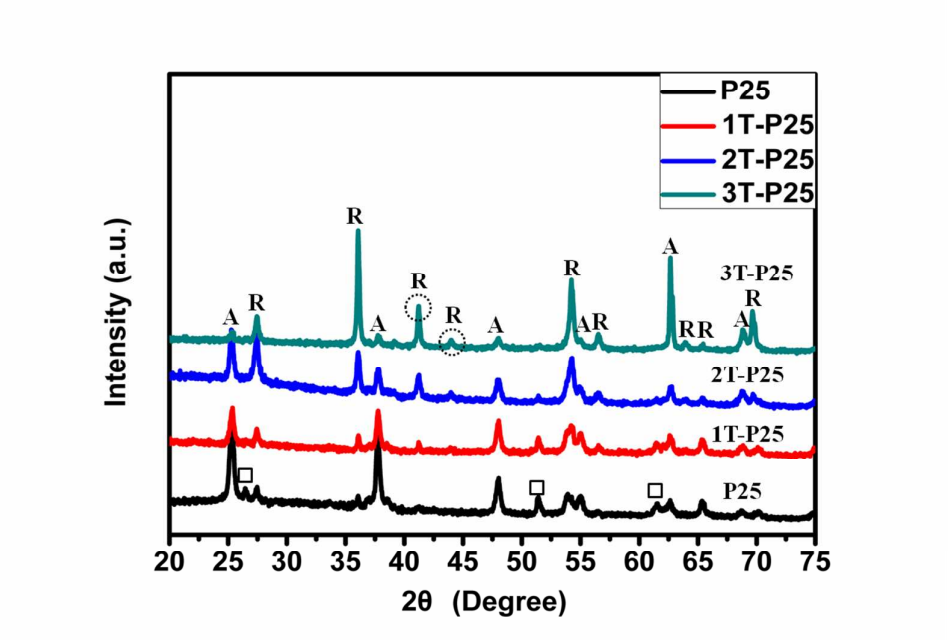

Fig. 1

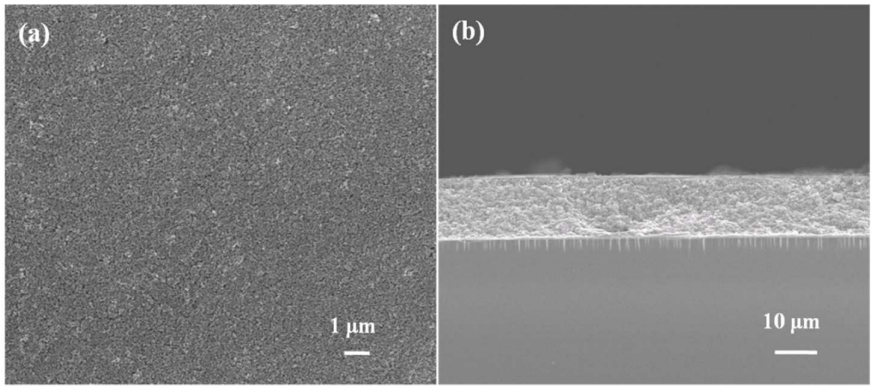

Fig. 2

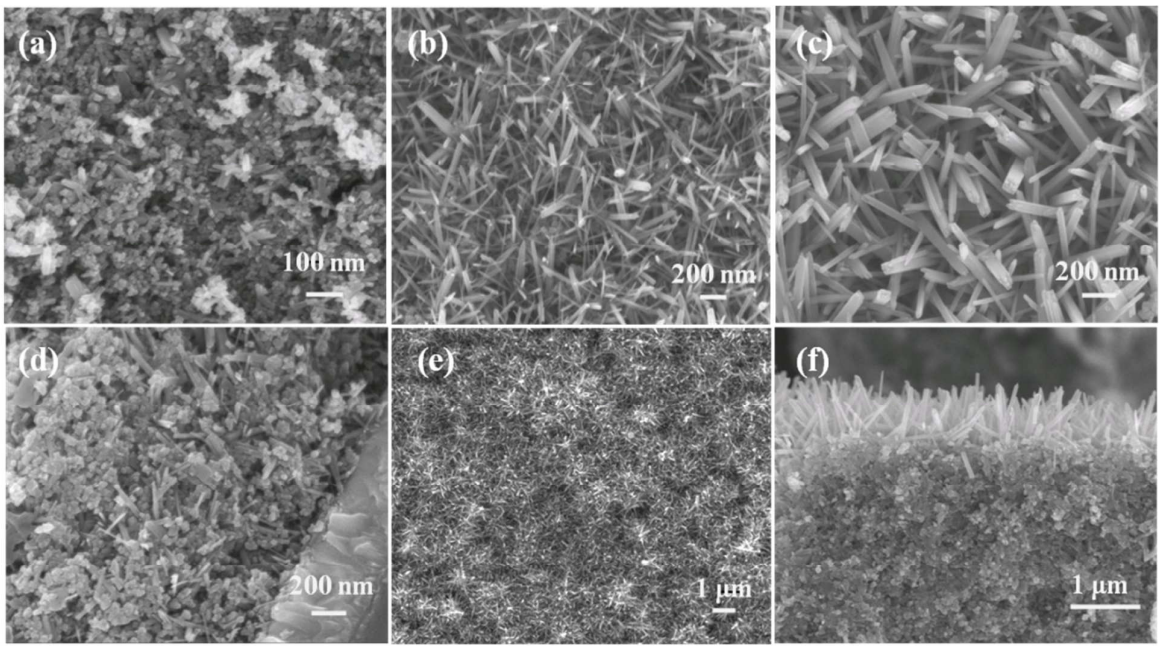

Fig. 3

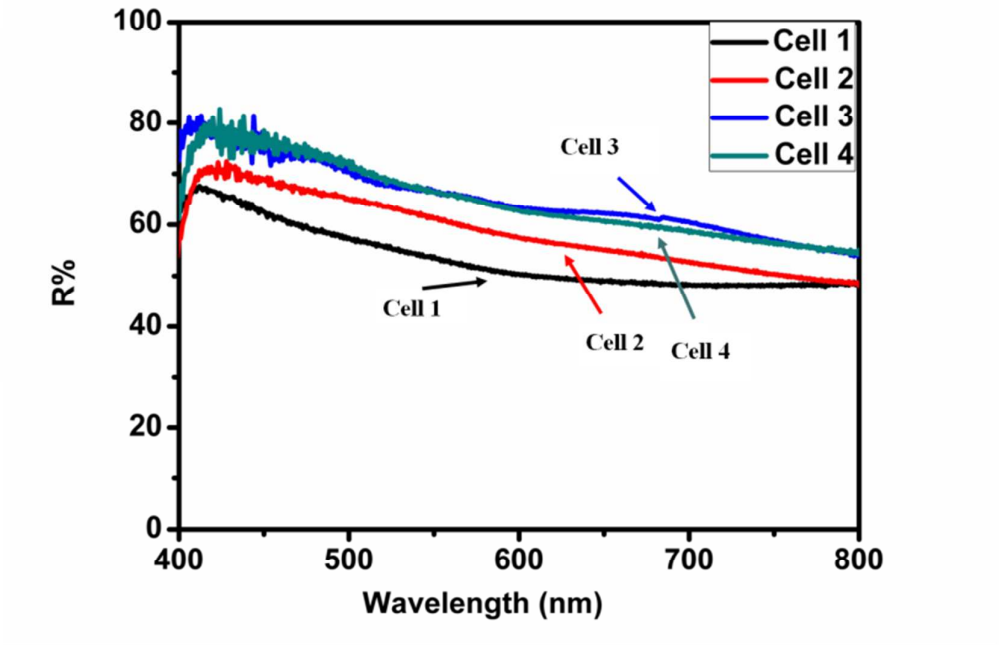

Fig. 4

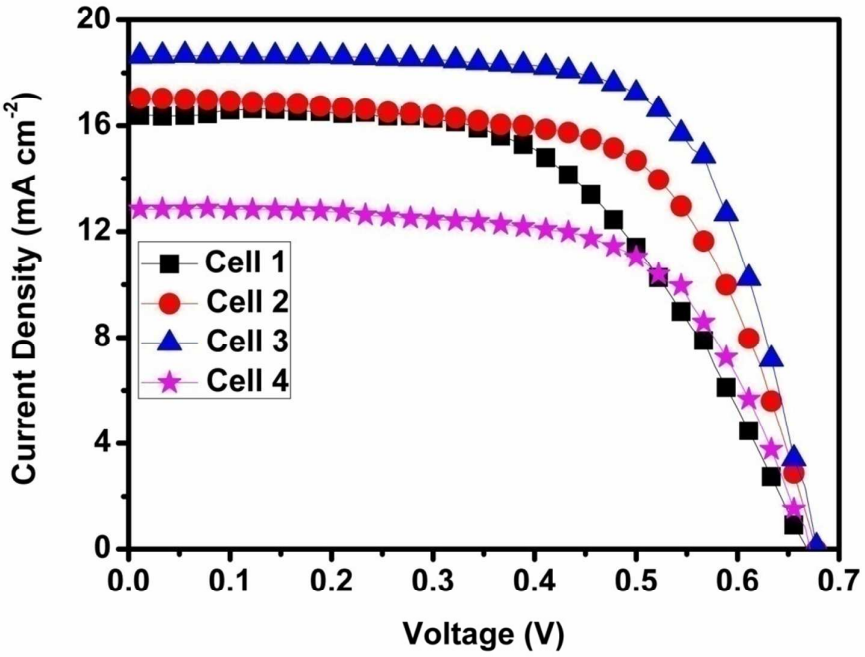

Fig. 5

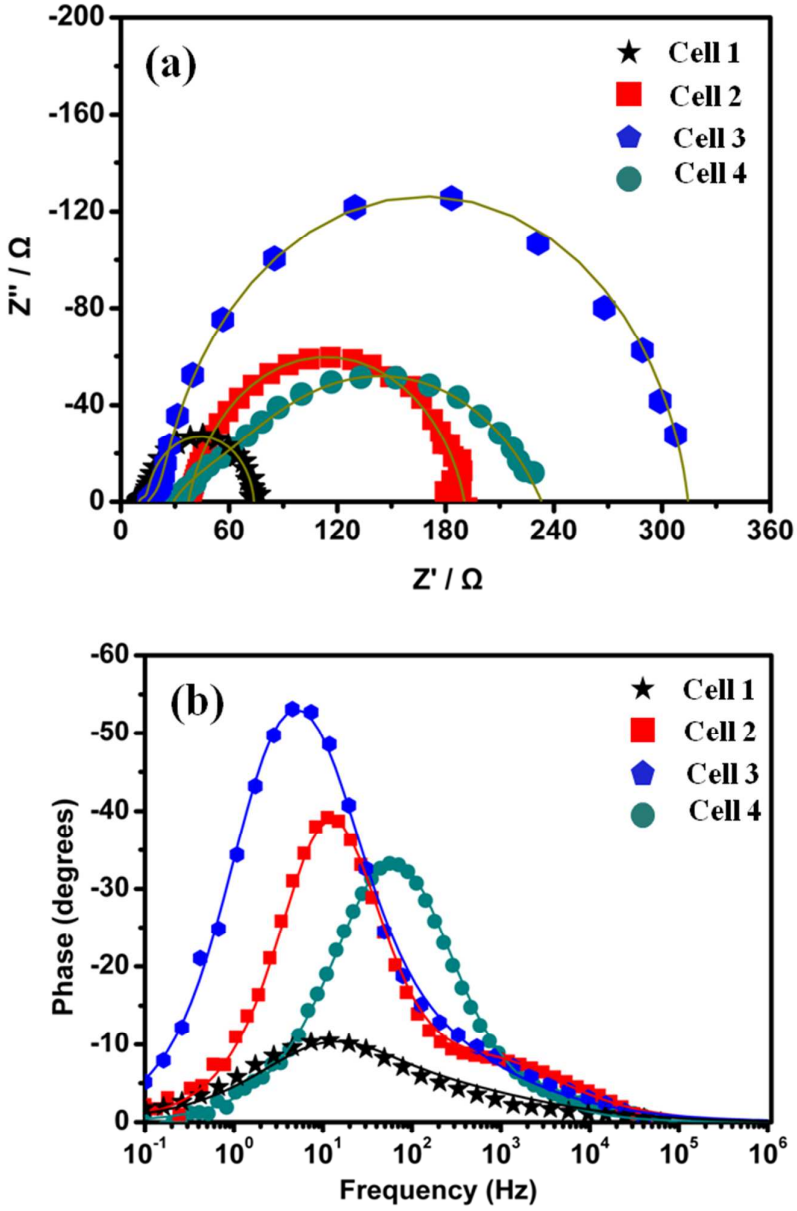

Fig. 6